Electrical Power and Energy Systems 120 (2020) 105992

Contents lists available at ScienceDirect

Electrical Power and Energy Systems

journal homepage: www.elsevier.com/locate/ijepes

A novel protection scheme for low voltage DC microgrid using inductance estimation

Morteza Shamsoddini[a], Behrooz Vahidi[a,*], Ramin Razani[b], Yasser Abdel-Rady I. Mohamed[b]

[a] Department of Electrical Engineering, Amirkabir University of Technology, Tehran 1591634311, Iran
[b] Department of Electrical and Computer Engineering, University of Alberta, Edmonton, AB, Canada

ARTICLE INFO

Keywords:
Back-up protection
Fault detection
Inductance estimation
Local measurement
Low voltage dc microgrid

ABSTRACT

Vulnerability of power electronic converters in DC microgrids when pole to ground and pole to pole fault occur necessitates using an effective fault detection and isolation. Most of the proposed fault detection methods use a communication system to exchange data among protection units, which could be an Achilles heel for the entire protection scheme. In this paper, fault detection based on estimation of equivalent inductance using simplified fault current equation is proposed. In the presented method, only local measurement is required and communication system is avoided due to reliability issues. In order to improve equivalent inductance estimation, an artificial line inductance (ALI) is implemented at both ends of each line. Since estimated equivalent inductance only depends on protection zone inductances including line inductance and ALIs, any change in topology of the microgrid does not affect operation of the protection scheme. By employing the proposed protection scheme, fault detection and isolation with a sampling frequency of 8000 Hz is achieved in less than 0.2 ms. A protection scheme should be able to disconnect the faulted section even if one of the main protection units fails; hence, by defining different protection zones for each protection unit, backup protection is realized. Eventually, to show significance of the proposed protection scheme, several case studies are investigated and results are compared with earlier studies.

1. Introduction

1.1. Motivation

Recent developments in power electronics (PE) and smart grids have convinced researchers that low voltage DC (LVDC) microgrid is a promising solution for future smart grids [1,2]. The LVDC microgrid has shown interesting features like high efficiency [3,4], easy connection of different power sources via PE converters [5] and increased transmission power capacity [6]. Moreover, these grids can be a great choice for electrifying remote communities, shipboards, spaceships and grids containing sensible loads in which power quality is critical [7,8]. However, power flow of DC environment inflicts new challenges, especially challenges which are related to protection issues. Since, the protection design considerations in DC systems are completely different compared to AC systems, the protection system in DC microgrids should be devised from the beginning.

On this point, a protection scheme in DC environment must have required characteristics to protect the LVDC microgrids properly against DC faults. On the obvious side, the protection scheme has to be as fast as possible to prevent probable damages to microgrid components, also it must only detach faulted part without interrupting operation of the microgrid. From a more challenging perspective, first, despite most of the available studies [9–12], the protection scheme settings should be independent of LVDC microgrid topology to avoid protection units failure caused by changes in the LVDC microgrid topology such as line, load or source outage. Second, cost efficiency of the protection scheme should be considered, since the number of consumers and their demanded power in the LVDC microgrid are low, protection schemes which require advanced protection units with expensive microprocessors and auxiliary apparatus like communication link are not cost efficient. Third, whereas the LVDC microgrids are possible choices for sensitive and important applications such as spaceships, shipboards, and data centers, reliability of protection schemes in these microgrids are of great importance. In the recent literatures, each or some of the mentioned characteristics of an advanced protection system for LVDC microgrids are investigated. However, there is a lack of a comprehensive scheme containing all the necessary characteristics, fast fault detection, independency to the microgrid topology, cost efficiency, selectivity and reliability in this area. Hence,

* Corresponding author.
E-mail address: vahidi@aut.ac.ir (B. Vahidi).

https://doi.org/10.1016/j.ijepes.2020.105992
Received 15 June 2019; Received in revised form 23 November 2019; Accepted 5 March 2020

this paper intends to design an efficient and advanced protection system for LVDC microgrids to satisfy all the mentioned requirements.

1.2. Literature review

In general, previous studies on LVDC microgrid protection can be classified into two main categories including communication-based and local measurement based protection schemes.

- Communication based protection scheme

The most well-known communication-based approaches are differential protection [13–15], event-based protection [10,16], centralized protection [17] and permission signal based protection [11,18]. Although these types of fault detection approaches provide appropriate protection for the desired area, they need a communication channel, which could be undesirably costly in low voltage microgrids. Moreover, this communication system might lose synchronization of data transmission; even the entire communication channel might be lost which would disable the protection schemes in fault detection and isolation.

- Local measurement based protection scheme

In [9], fault detection based on analysis of local measurement has been proposed which detects faults based on predefined thresholds of first and second current derivatives. The defined thresholds highly rely on grid topology. In this case, if topology of the microgrid changes, the protection scheme might not be able to detect the faults any more. In [12], low impedance fault has been detected using well-known over current method, and discrete wavelet analysis is employed to detect voltage transient generated by implemented passive elements in relay for high impedance fault detection. Both approaches for low and high impedance faults use local information. However, designed resonance frequency of passive components could change as components wear-out, as a result of which the relay cannot detect faults. Moreover, this approach imposes high computational burden, which requires powerful processors making it uneconomical for low voltage DC microgrids. Inspired by distance protection in the AC grid, a fault detection method has been experimentally evaluated on LVDC microgrid in [19], which relies on coordination between power source converters and bus segmenting contactors. In this approach, the protection units based on time-trip curve as a function of calculated resistance decide whether the trip signal should be sent or not. Implementation of this approach highly depends on PE converters of the grid to limit the fault current. Moreover, in case of a high impedance fault, the calculated resistance might not be below the threshold, thus the fault is not detected.

1.3. Contribution

In this paper, a novel protection scheme based on fault current characteristics is proposed for LVDC microgrids. In this method, first, the equivalent inductance is estimated by local measurement of the fault current. Second, the protection units detect the fault and disconnect the faulted section in less than 0.2 ms based on inductance-time diagram. Eventually, in order to improve reliability of the proposed scheme, back-up protection is realized by defining second zone protection in inductance-time diagram. The presented protection scheme offers fast fault detection, communication-less algorithm, backup protection realization and independency from microgrid topology. In order to verify response time, sensitivity, selectivity and backup protection of the presented method, different scenarios are studied in a five bus ring LVDC microgrid. At the end, a comprehensive comparison is made among some earlier studies and the proposed fault detection method.

1.4. Organization of the paper

Rest of this paper is organized as follows: formulization of the fault current in DC microgrid, the proposed fault detection method, and associated protection scheme are presented in Section 2. In Section 3, simulation results and analysis are expressed. A comparison of the proposed method with earlier approaches is presented in Section 4. Finally, the paper is concluded in Section 5.

2. Proposed non-unit protection system

Despite of unit protection schemes, non-unit protection schemes are able to provide backup protection for DC microgrids, and they will take action if a neighboring protection unit fails to operate [20]. This section presents a non-unit protection method to achieve an effective protection scheme based on the fundamental characteristics of fault current. To make understanding of the proposed non-unit protection scheme easier, fault current analysis in DC environment is provided in the following, which is the basis of proposed fault detection scheme.

In DC microgrids, maximum allowable response time of protection units is mainly determined based on thermal endurance of switches of voltage source converters (VSC). This could be explained by fault current analysis. When a fault occurs, switches of the converters are blocked to prevent possible damages. The DC bus capacitor filter acts as a DC voltage source and discharges via an equivalent RLC circuit (Fig. 1a). The natural response of this circuit in Laplace-domain can be expressed as:

$$I(s) = \frac{v_C(0)/L_{eq} + s i_L(0)}{s^2 + \frac{R_{eq}}{L_{eq}} s + \frac{1}{L_{eq}C}} \tag{1}$$

where $i_L(0)$ and $v_C(0)$ are line current and DC voltage of the bus prior to fault, respectively. Also, $R_{eq}$and L_{eq} are equivalent resistance and inductance of the fault circuit. The equation corresponding to fault current can also be expressed in the time-domain as presented in (2).

$$I(t) = \frac{v_c(0)}{L_{eq}(p_2 - p_1)}(e^{-p_1 t} - e^{-p_2 t}) + \frac{i_L(0)}{(p_2 - p_1)}(-p_1 e^{-p_1 t} + p_2 e^{-p_2 t}) \tag{2}$$

where $\boldsymbol{p}_1$ and $\boldsymbol{p}_2$ can be calculated as:

$$p_1, p_2 = \alpha \pm \omega \tag{3}$$

In which $\alpha = R_{eq}/2L_{eq}$, $\omega = \sqrt{\alpha^2 - {\omega_0}^2}$ and $\omega_0 = 1/\sqrt{L_{eq}C}$. If $\alpha^2 < {\omega_0}^2$, the current response would be under-damped, if $\alpha^2 > {\omega_0}^2$, the current response is over-damped and in case of $\alpha^2 = {\omega_0}^2$, the current is critically damped. The time taken for the under-damped and over-damped currents to reach their peak values can be calculated as:

$$t_{ud}^{p} = \frac{1}{\omega_0}\tan^{-1}\left(\frac{\omega_0}{\alpha}\right) \tag{4}$$

$$t_{od}^{p} = \frac{\ln p_2/p_1}{p_1 - p_2} \tag{5}$$

t_{ud}^{p} and t_{od}^{p} are important parameters of the protection system, because it

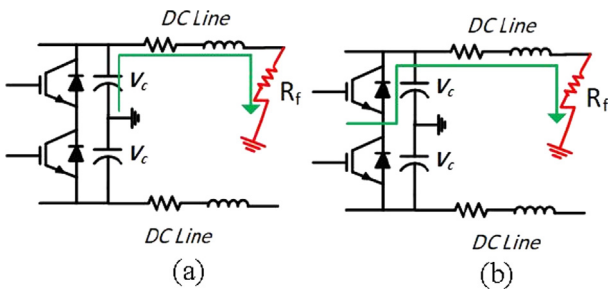

Fig. 1. Fault equivalent circuit (a) First stage (b) Second stage.

must detect and disconnect the faulty section before the fault current reaches its peak value, so that VSC damage and DC load voltage collapse are prevented. If the faulty section is not disconnected before t_{od}^{p} andt_{ud}^{p}, voltage of the DC bus capacitor would be lower than the AC side and the fault current enters second stage. In this stage, since the voltage of the DC bus is lower than the AC side, freewheeling diodes in the VSCs act like a three-phase rectifier and let the AC side contribute to the fault current (see Fig. 1b). This current which flows through the diodes to the DC side is several times higher than the rated value and can cause catastrophic damages to VSC components [20]. Therefore, it is indisputable that the protection system must detach the faulted section before the second stage onset.

The key findings from this analysis with simplifying assumptions are employed to propose a novel fault detection method in the next subsection and develop an effective protection scheme in the rest of this section.

2.1. Fault detection

In the fault current, the contribution of the initial line current in the LVDC microgrid is negligible compared to the DC bus voltage. Hence, in this study, effect of initial current of the fault path inductance is neglected regarding DC bus capacitor voltage [18,20]. Thus, the fault current equation can be rewritten as follows:

$$I(t) = \frac{v_c(0)}{L_{eq}(p_2 - p_1)}(e^{-p_1 t} - e^{-p_2 t}) \tag{6}$$

Using McLaurin series, the exponential terms of (6), $e^{-p_1 t}$ and $e^{-p_2 t}$, can be approximated by (7) and (8), which are valid for a very short time after the fault ($t = 0^{+}$).

$$e^{-p_1 t_i} \simeq 1 - p_1 t_i \tag{7}$$

$$e^{-p_2 t_i} \simeq 1 - p_2 t_i \tag{8}$$

where t_i is the time at which data is sampled after the fault. By substituting (7) and (8) in (6), the following equation can be derived:

$$I(t_i) \simeq \frac{v_c(0)}{2L_{eq}\omega}(2\omega t_i) \tag{9}$$

t_i's are determined by sampling frequency, i.e., if the sampling frequency is 8000 Hz, the first sample is taken at $1/8000 = 125$ μs after the fault incident and the second sample is taken 125 μs later at 250 μs after the fault. Therefore, by generalizing the relationship between t_i's and sampling frequency, the following equation can be obtained:

$$t_i = \frac{i}{f} \tag{10}$$

In which, i is the number of sampled data after fault occurrence and f is the sampling frequency. By substituting (10) in (9), the equivalent inductance under fault condition can be calculated as:

$$L_{eq} \simeq \frac{v_c(0)}{I(t_i)} \times \frac{i}{f} \tag{11}$$

Using (11), the equivalent inductance observed by each protection unit can be estimated. When a fault occurs along the line, the associated protective devices (PDs) measure smaller inductance compared to the entire line inductance. Consequently, by defining a threshold for estimated inductance, faults along DC cables can be detected. But, first, the time after fault incidence in which approximations are valid should be studied.

2.2. Enhancing the approximation validity using ALI

Although, the McLaurin series simplifies (6) to (11) at $t = 0^{+}$, the obtained equation is valid for a very short time after fault incidence. Due to the approximation of $e^{-p_1 t}$ and $e^{-p_2 t}$ by $1 - p_1 t_i$ and $1 - p_2 t_i$, precision is lost significantly during the time after fault occurrence. Thus, it is necessary to determine the time after fault in which approximation is still valid. This could be done by considering and analyzing error terms of Taylor series. In general, for every given function $f(x)$, the following equation can be derived.

$$f(x) = R_n(x) + E_n(x) \tag{12}$$

In which, $\boldsymbol{R_n(x)}$ represents the first n terms of Taylor series of $\boldsymbol{f(x)}$ around $\boldsymbol{a}$, and $\boldsymbol{E_n(x)}$ is the approximation error of $\boldsymbol{f(x)}$ being approximated by Taylor series $\boldsymbol{R_n(x)}$ [21]. The following equation can be expressed for $\boldsymbol{R_n(x)}$ and $\boldsymbol{E_n(x)}$:

$$R_n(x) = \sum_{i=0}^{n} \frac{f^{(i)}(x)}{i!}(x - a)^i \tag{13}$$

$$E_n(x) = \frac{f^{(n+1)}(\alpha x)}{(n+1)!}(x - a)^{(n+1)} \tag{14}$$

In (14), α is used to maximize the value of $(n+1)th$ derivative of $f(x)$ in the range of $x \le \alpha \le a$. In fact, this parameter helps to find the upper limit of (14) as follows:

$$E_n(x) \le \frac{M}{(n+1)!}(x - a)^{(n+1)} \tag{15}$$

Now, by using (15), the approximation in (7) and (8) can be analyzed. The error of (7) is calculated in following equation.

$$E_1(p_1 t_i) = \frac{(e^{-p_1 t_i})'' * (p_1 t_i)^2}{2!} \tag{16}$$

where $(e^{-p_1 t_i})''$ is the second derivative of $e^{-p_1 t}$ around zero and its maximum value is 1. Considering an upper limit (ε) for (16), (17) and (18) can be expressed.

$$\frac{(p_1 t_i)^2}{2} \le \varepsilon \tag{17}$$

Eventually, by substituting the equivalent term of p_1 based on circuit parameters, (18) can be written.

$$\left(\frac{R_{eq}}{2L_{eq}} + \sqrt{\left|\left(\frac{R_{eq}}{2L_{eq}}\right)^2 - \frac{1}{L_{eq}C}\right|}\right) * t_i \le \sqrt{2\varepsilon} \tag{18}$$

In the worst-case scenario, in which fault occurs near the DC bus (very small inductance) and the fault resistance has its maximum value (0.6 Ω), the time in which approximations are valid has its minimum value. For example, consider a fault occurs at 5 m away from bus1 along the line 1–2 in the shown microgrid (Fig. 2) with given parameters in the Table 1. By calculating the fault path inductance from bus1 and considering the equivalent fault resistance of 0.6 Ω and $\varepsilon = 0.3$ percent, the time in which approximations are valid is 0.3 *us* after fault incidence. Since efficient operation of the proposed fault detection requires calculating the equivalent inductance from (11) for some sampled data after the fault, the sampling frequency must be increased to hundreds of Hz, which is not possible. Another solution is to add small inductors to both ends of the line. This technique can extend the time in which approximations are valid without increasing the sampling frequency, which is highly beneficial in the worst-case scenario. It is noteworthy that adding these inductors to both ends of the line do not increase total loss of the microgrid and only affect the fault current dynamic. Since the added inductors act like a specific length of the line with a very low resistance, this technique is called artificial line inductance (ALI). To elucidate it more, consider the mentioned worst-case scenario which the fault resistance is 0.6 Ω, ε is 0.3 percent, fault location is 5 m away from bus1 and sampling frequency is 8 kHz. The proposed method takes two samples to detect the fault, which means that the time in which approximations are valid must be at least 0.25 ms. By substituting these values in (18), the ALI value, which should be added to both ends of the line is calculated as 0.1mH.

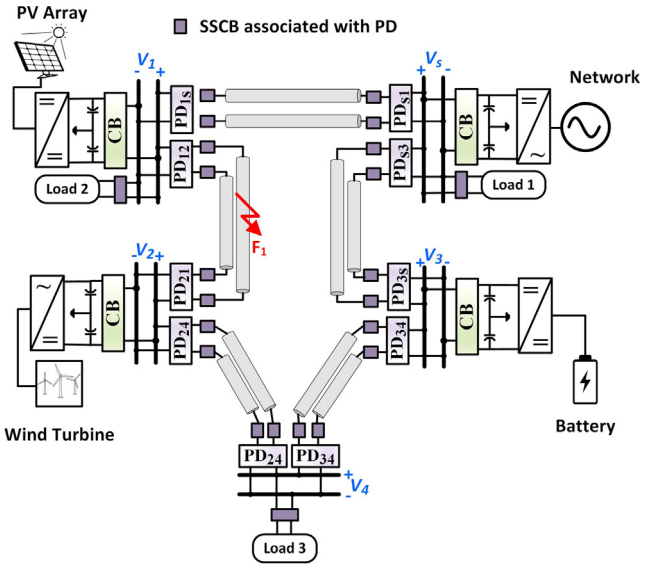

Fig. 2. Studied DC microgrid.

Table 1
Main parameter of the DC microgrid.

Name	Value
Grid Voltage	*400 V DC*
Battery	*130 V, 0.4 kAh*
Solar panel	V_{mppt} = *29 V* I_{mppt} = *7.35 A at STC*
Wind turbine	*400 kW*
Cable resistance	*0.125 Ω/km*
Cable inductance	*0.232 mH/km*
All cable length	*0.5 km*
DC link capacitor	*12.5 mF*
Load	*Constant impedance load 250 kW*

The time at which fault current reaches its peak value (t_{peak}) for different locations of fault f_1 is analytically calculated in Table 2. The results demonstrate that as fault path inductance increases, fault current transients become slower. Consequently, sampling frequency could be decreased. In this paper, it is assumed that sampling period should be at least less than half of minimum t_{peak}. Also, the relationship between sampling frequency, ALI and equivalent fault path resistance is presented in Fig. 3.

2.3. Setting inductance threshold for PDs

When fault happens in the DC microgrid, inductance of healthy lines can be neglected compared to inductance of the faulty line. Thus, the equivalent inductance which is sensed by each PD corresponds to the inductance between PD and fault point [19]. In this regard, PDs' inductance threshold for fault detection can be calculated using (19), which is equal to total inductance value under fault condition between two PDs obliged to protect a line.

$$L_{threshold} = 2L_{ALI} + L_{cable} \tag{19}$$

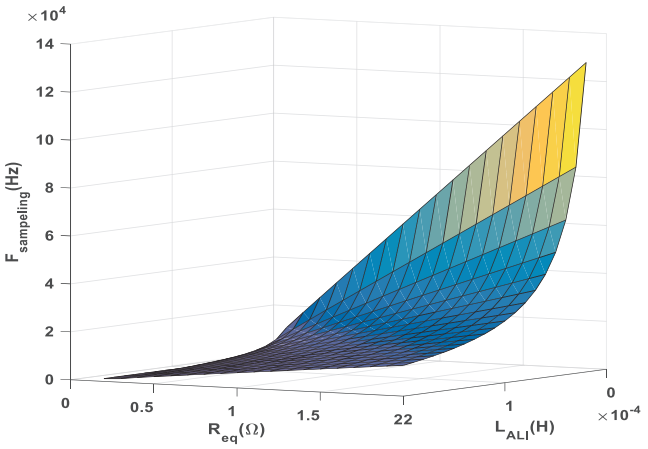

Fig. 3. Sampling frequency with respect to the equivalent resistance and ALI.

In which, L_{ALI} is the value of ALI and $L_{cable}$is the line inductance. $L_{threshold}$ is the inductance threshold.

2.4. Protection algorithm

The current of the lines is monitored permanently by PDs, which are installed at both ends of the microgrid lines as depicted in Fig. 2. These PDs have been installed for microgrid protection with three different functions including start-up, fault detection and isolation, and back-up protection. Operation of each function in the proposed protection scheme is explained in the following.

2.4.1. Start-up function

In the proposed protection scheme, the start-up function is based on amplitude of the line current, i.e., if the measured line current exceeds the threshold value, the fault detection function is triggered. This threshold is determined based on the rated power of the microgrid and loads. In general, the threshold of the line current ($I_{pick-up}$)should be higher than maximum current of the line (I_{L-max}) when the demanded power is maximum and less than minimum fault current (I_{f-min}), simultaneously.

$$I_{L-max} < I_{pick-up} < I_{f-min} \tag{20}$$

However, under normal operation, sometimes the minimum fault current is lower than the maximum line current. In this case, the line current threshold is set to I_{f-min}which might activate the fault detection function under heavy load changes.

2.4.2. Fault detection and isolation function

The fault detection function is triggered when the amplitude of the line current exceeds the predefined threshold. For this function to detect the fault and send a trip signal to its related SSCB, two conditions have to be satisfied.

- *1st Zone Inductance Threshold:*

First, the equivalent inductance from the PD view is calculated using (11). This has to be lower than the first zone inductance threshold

Table 2
Minimum required frequency (f_{min}) respect to its t_{peak} seen by PD_{12} for different fault f_1 location.

Distance from bus1 (m)	50		100		150		200		250	
Time (ms) / Frequency (kHz)	t_{peak}	f_{min}	t_{peak}	f_{min}	t_{peak}	f_{min}	t_{peak}	f_{min}	t_{peak}	f_{min}
Without ALI	0.019	105.3	0.039	51.3	0.058	34.5	0.077	26	0.096	20.8
With ALI	0.35	5.7	0.36	5.6	0.38	5.3	0.4	5	0.42	4.8

$L_{1stzone}$, which is equal to $L_{threshold}$ determined in the previous subsection. Since the equivalent inductance of both positive and negative lines are calculated simultaneously, all fault types, positive pole to ground, negative pole to ground and pole to pole can be detected. If one of the PDs calculated inductances is lower than $L_{1stzone}$, the trip signal is transmitted only to the corresponding SSCB. In case that calculated equivalent inductance of both positive and negative poles is lower than $L_{1stzone}$ which indicates pole to pole fault, the trip signal is sent to the SSCBs of both negative and positive lines.

- *Current Direction:*

The fault current direction must also match the predefined direction. In case of positive pole to ground fault, the fault current exits the DC bus through the positive line. In case of negative pole to ground fault, the fault current enters the DC bus. When pole to pole fault occurs, the fault current enters the DC bus through the negative line and exits via the positive line. Consequently, the second condition is satisfied if the current measured by PD matches one of the above cases.

2.4.3. Back-up function

When a fault is detected and the trip signal is sent to the corresponding SSCBs of the faulted line, the PDs still monitor the line current to ensure that SSCBs work properly. If the line current is not reduced to zero after a specific time, the back-up function is activated. In this case, the PDs which have the following conditions are authorized to send the trip signal to their SSCBs.

- *2nd Zone Inductance Threshold:*

The calculated equivalent inductance has to be in the 2nd zone as shown in Fig. 4. The inductance threshold in the 2nd zone $L_{2ndzone}$ can be calculated as follows:

$$L_{2ndzone} = 2L_{ALI} + L_{cable}^{2nd} + L_{1stzone} \quad (21)$$

In which, L_{cable}^{2nd} is the adjacent main protection line inductance. As mentioned in Section 2, the fault current in the VSC-based LVDC microgrid should be blocked before the second stage, which starts after t_{ud}^{p} or t_{od}^{p}. These times for the extreme fault case in the studied microgrid (Fig. 2) are obtained around 2 ms (calculation is based on presented parameters in Table 1). Thus, the first and second zone protection operation times are determined as 1 and 2 ms, respectively (Fig. 4).

- *Current Direction:*

This condition is the same as what was described for fault detection and isolation function. Whenever the fault current matches the predefined case, this condition is satisfied, and if the measured inductance is lower than the second zone threshold, the trip signal is sent to the corresponding SSCBs.

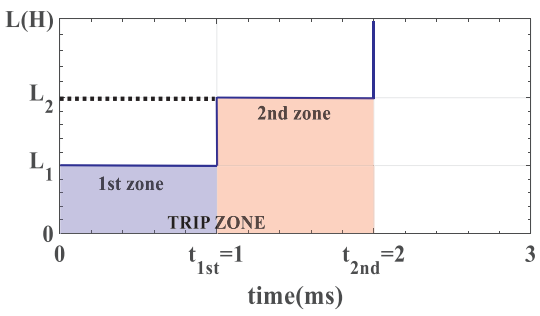

Fig. 4. Inductance-time characteristics of different zones.

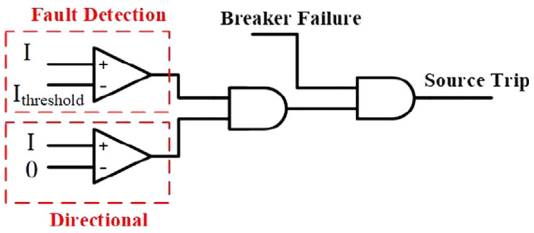

Fig. 5. Logic circuit for generation of trip signal for power sources.

2.4.4. Power source trip signal generation

For the backup protection to be fully realized, a different approach is required for the backup function of PDs connected to the power source. To explain it further, the following example is presented. Consider that fault f_1 occurs (see Fig. 2) and SSCB of PD_{12} fails to operate, thus the back-up function of the protection scheme will be activated. When SSCB of $PD_{s1}$is disconnected, the fault point is still fed by the power source connected to bus1. Therefore, the corresponding PD has to detach the power source from bus1. The corresponding trip is generated by the logic circuit of Fig. 5. As shown, the power source trip signal is produced based on magnitude and direction of the fault current and breaker failure signal. If the measured fault current in one PD does not decay below a predefined threshold within 1 ms (first zone operation time), that PD would perceive that its SSCB has failed. In this situation, it sends the breaker failure signal to the PD connected to the power source in the same DC bus. Consequently, the power sources are prevented from contribution in the fault current.

2.5. Implemented algorithm in each PD

The proposed protection algorithm is presented in Fig. 6. In this algorithm, if the line current exceeds the predefined threshold $I_{pick-up}$, the fault detection and isolation function are triggered. The equivalent inductance of each pole line is calculated using (11), if it is lower than $L_{1stzone}$ and the current direction matches the predefined direction, the trip signal is sent to the corresponding SSCB. The PDs monitor the line current after sending the trip signal to ensure that it has subsided to zero. If the fault current has not decreased to zero after a specific time, the backup function is activated. Moreover, the associated PD of the failed SSCB sends the breaker failure signal to PD of the power sources which are connected to the same bus as failed SSCB is connected. Consequently, the power sources are disconnected from the grid. Meanwhile, other PDs which have calculated equivalent inductance less than $L_{2ndzone}$, and their currents direction satisfy the predefined cases, the trip signal is sent to corresponding SSCBs.

3. Simulation studies and analysis

In this section, several case studies including change in microgrid topology, different types of fault, back-up protection under breaker failure, and fault in noisy environment are investigated to verify performance of the proposed protection scheme. These studies are conducted in the loop type LVDC microgrid illustrated in Fig. 2 (control scheme is described in the [18]). Also, to evaluate the proposed protection scheme performance on the other topologies, a case study with distribution topology is considered. Finally, cyber-physical risk assessment for the proposed protection scheme is presented.

It should be noted that inductances estimated by PD which protect the LVDC microgrid in anti-clockwise direction and clockwise direction are presented as $L_R$and L_L, respectively. In the figures, *Lpij* and *Lnij* are the positive and negative pole inductances estimated by PD_{ij}. The main design parameters of the proposed protection scheme are given in Table 3.

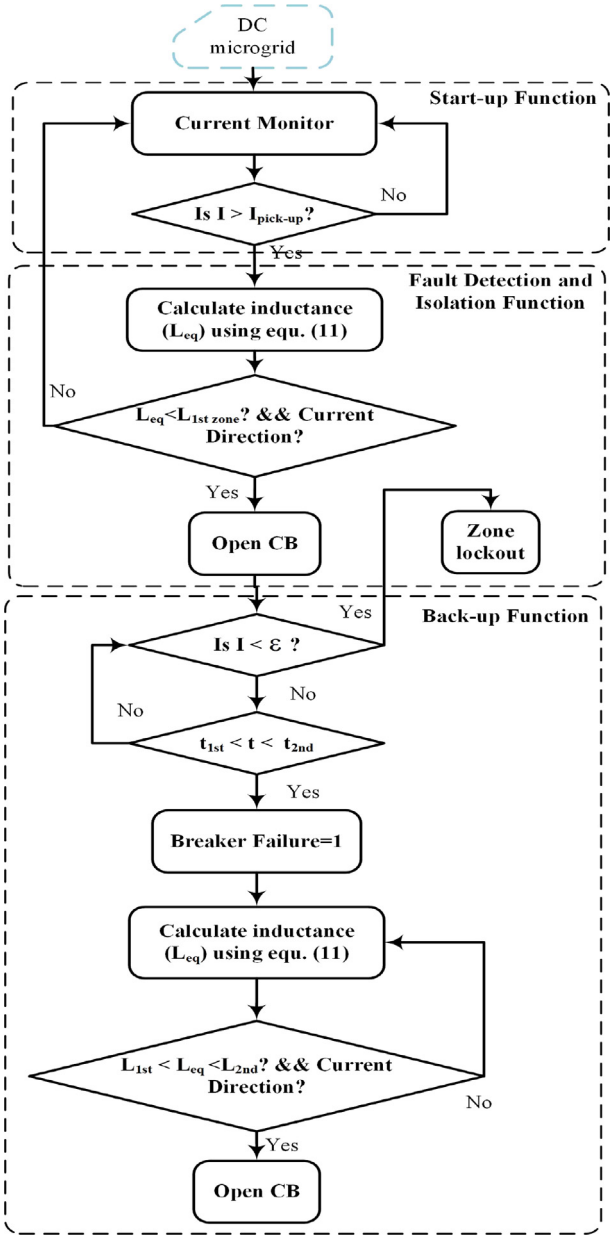

Fig. 6. The proposed algorithm for fault protection.

Table 3
Parameters of the protection scheme.

Name	Value
$I_{pick-up}$	*50 A*
ALI	*0.1 mH*
1st zone threshold	*0.316 mH.*
2nd zone threshold	*0.632 mH*

3.1. Change in microgrid topology

In order to show fault discrimination capability of the protection scheme with other incidents such as load changes or sudden line outage, three different scenarios are considered; increase in demanded power, load elimination and sudden disconnection of a line. First, a 20 kW load is added to bus4 at t = 2.5 s. Then, this load is disconnected at t = 5 s. Finally, the line between bus3 and bus4 is disconnected at t = 7.5 s. The DC bus voltage and line current of the microgrid are

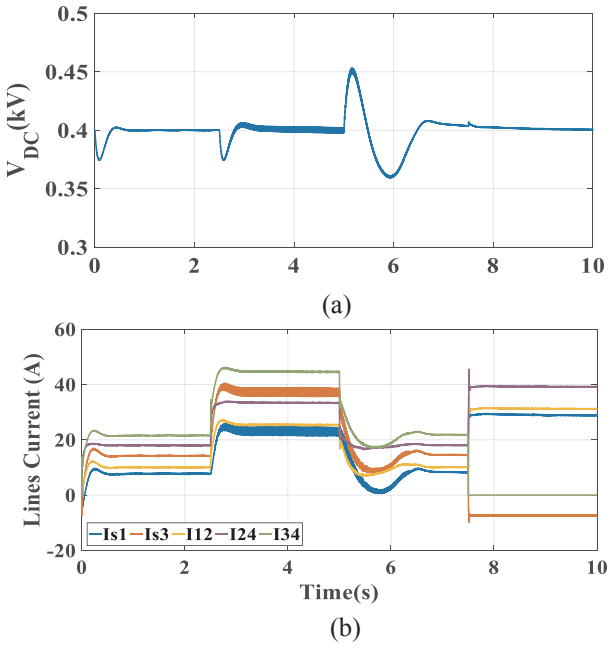

Fig. 7. Change in microgrid topology (a) slack bus voltage (b) lines current.

presented in Fig. 7a and b, respectively. As can be seen, the microgrid is able to continue its operation and maintain DC bus voltage quickly after each disturbance and no fault is detected by any PD.

3.2. Evaluating of the ALI method effectiveness

To show the effectiveness of ALI, two different scenarios are investigated. In one of the scenarios, the ALI method has implemented in both ends of the line, while in the other scenario, the ALI is not used. In both scenarios, line to ground fault f_1 at the distance of 200 m from bus1 (300 m from bus2) with equivalent fault path resistance of 0.6 Ω at $t = 1s$ is simulated. Fig. 8 illustrates results of these two scenarios. As Fig. 8a shows, when the ALI method is employed, protection devices (PD) can detect the fault and disconnect the faulted line. However, when the ALIs are removed, the PDs are not able to detect the fault. Estimated inductances of the two case studies are presented in Fig. 8b and c. Fig. 8b shows the scenario which ALI method is employed. The, estimated inductances by PDs of the faulted line are less than the fault threshold. However, in the other scenario as shown in Fig. 8c, the estimated inductances by PDs are greater than fault threshold. Without using ALI method, sampling frequency should be increased to enable PDs to detect faulted part.

3.3. Different types of faults

3.3.1. Pole to pole fault

In this case study, a pole to pole fault f_2 occurs at 200 m of the slack bus (300 m from bus3) at $t = 3$ s. The calculated equivalent inductances by each PD after the fault in both positive and negative lines are presented in Fig. 9. In this regard, PD_{3s} and PD_{s3} in both positive and negative lines calculate 0.15233mH (Fig. 9a) and 0.17682 mH (Fig. 9b), respectively. Thus, these units detect the fault and issue the trip signal to the corresponding SSCBs to disconnect line 3-s. Due to this fact, the fault current in both positive and negative line 3-s is decayed to zero as depicted in Fig. 9c.

3.4. Fault with high resistance

The proposed protection scheme is designed for faults with resistance of 0.6 Ω; however, in this case, the fault with a resistance of

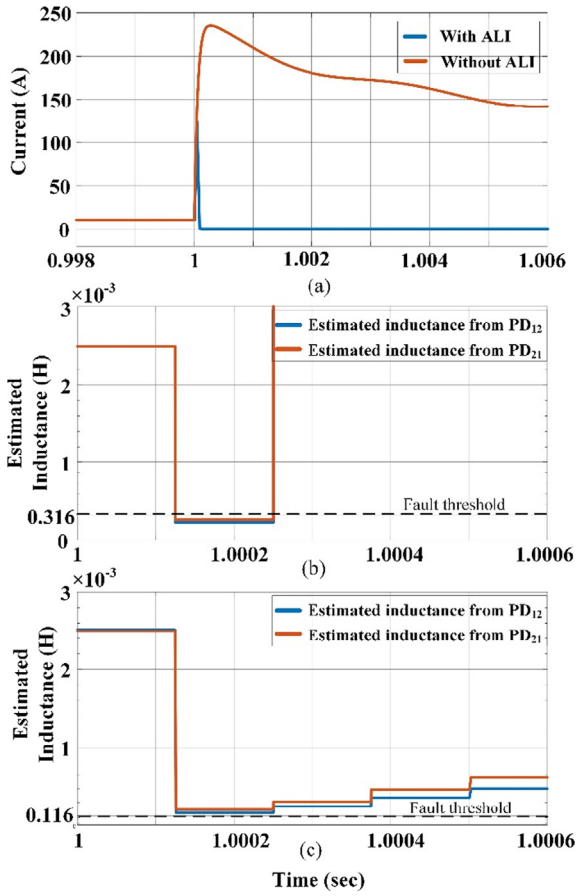

Fig. 8. ALI effectiveness validation (a) faulted line current (b) inductance estimated of faulted line by PDs with ALI employing (c) inductance estimated of faulted line by PDs without ALI employing.

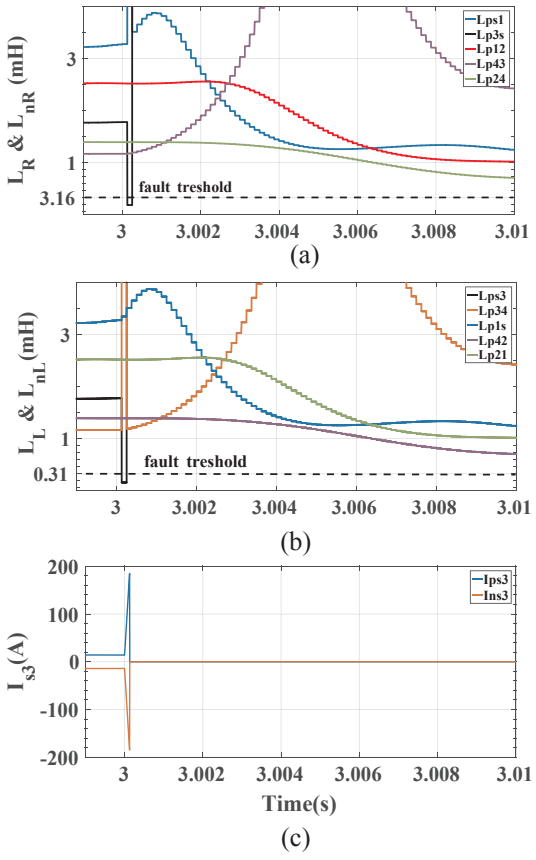

Fig. 9. Pole to pole ground fault f_2 (a) inductances estimated on positive and negative poles byPD_{s1}, PD_{3s}, PD_{12},PD_{43} and PD_{24} (b) inductances estimated on positive and negative poles byPD_{1s}, PD_{3s}, PD_{21},PD_{34} and PD_{42}(c) positive and negative line 3-s current.

2 Ω is also investigated. In this regard, a positive pole to ground fault f_3 with resistance of 2 Ω occurs at the distance of 50 m from bus4 (450 m from bus2) at $t = 3$ s. The inductances calculated by PDs are shown in Fig. 10. The protection units of line 2–4, PD_{24} and PD_{42}, compute an inductance of 0.31486 mH (Fig. 10a) and 0.13194 mH (Fig. 10b), respectively, which are lower than $L_{1stzone}$. Therefore, line 2–4 is disconnected by their commands and the fault current is cut off within 0.2 ms (Fig. 10).

3.5. Back-up protection

To verify operation of the back-up protection in the proposed protection scheme, a positive pole to ground fault f_4 is imposed at 200 m on bus1 (300 m from slack bus). In this scenario, although the equivalent inductance calculated by PD_{s1} is smaller than the first zone threshold as shown in Fig. 11a, it is assumed that SSCB of PD_{s1} fails to operate and disconnects the line due to technical problems, thus the protection scheme enters back-up protection. In this situation, other PDs are responsible to provide back-up protection based on the rules mentioned in Section 2. As the test microgrid of Fig. 2 shows, if SSCB of PD_{s1} fails, PD_{3s} is responsible to detect the fault and disconnect the faulty line. As shown in Fig. 11a, the inductance calculated by PD_{12} also complies with the second zone inductance-time characteristic condition, but because it does not satisfy the current direction condition, it is not allowed to send the trip signal to its SSCB. It is also important to disconnect the power source from the slack bus to stop feeding the fault. Eventually, before the second stage of the fault current, lines 1-s and s-3 are disconnected in less than 2 ms as depicted in Fig. 11b.

3.6. Noise effect

In order to have a closer look at the proposed protection scheme, its operation in the presence of noise is investigated. Environmental conditions can create noise in communication systems and measurement equipment, which could affect the whole protection system. In the proposed scheme, the need for communication system is eliminated. Thus the only vulnerable part is the measurement equipment. The power distribution coefficient of noise in measurement can be considered as a Gaussian distribution [22]. To analyze it further, the operation of the proposed protection scheme in the presence of 20 dB signal to noise ratio when fault f_5 with 0.6 Ω resistance at a distance of 350 m from bus3 (150 m from bus4) is imposed at t = 3 s is studied. As shown in Fig. 12, noise does not affect the protection scheme and PDs of line 4–3 are still able to detect and disconnect the faulty line.

3.7. Evaluation of the proposed protection scheme on a practical DC distribution system

In this subsection, the loop type DC microgrid of Fig. 2 is converted to a DC distribution system [23] as illustrated in Fig. 13. To avoid recalculation of the ALI value, it is assumed the cable characteristics of the distribution test system is the same as loop type microgrid of Fig. 2, which are given in Table 1. Furthermore, the network and solar panels are the only power sources and the other power sources are replaced with new loads.

At the instance of t = 1 s, the DC distribution system is tested for the positive line to ground fault *f* which is 100 m away from bus2 (400 m from bus5) with the fault resistance of 0.8 Ω. PD_{25} and PD_{52}, are the protection units of the faulted line, and they estimate the fault path

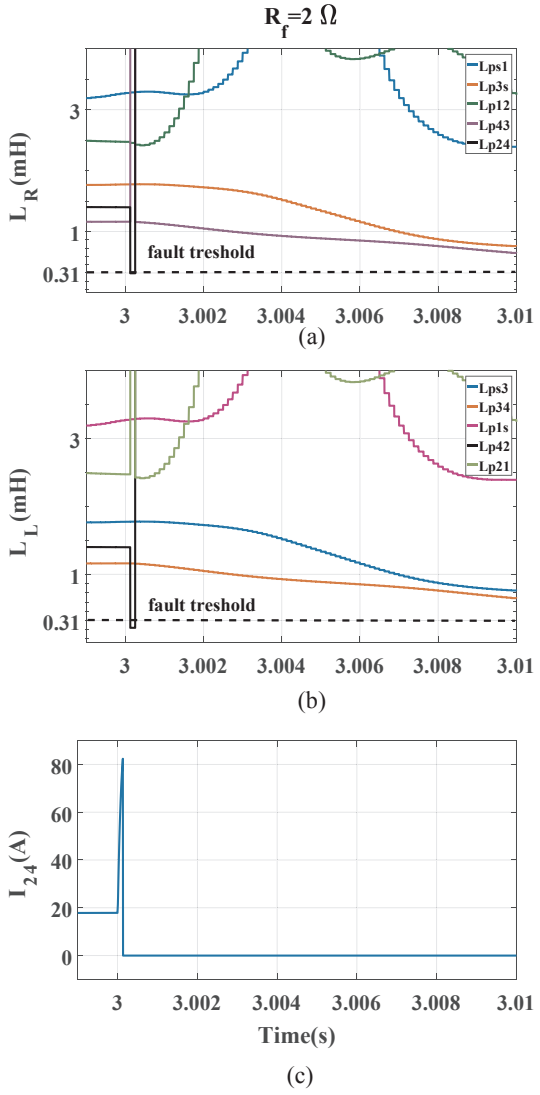

Fig. 10. Positive pole to ground fault f_3 with $R_f = 2\ \Omega$ (a) inductances estimated by PD_{s1}, PD_{3s}, PD_{12},PD_{43} and PD_{24} (b) inductances estimated byPD_{1s}, PD_{3s}, PD_{21},PD_{34} and PD_{42} (c) line 2–4 current.

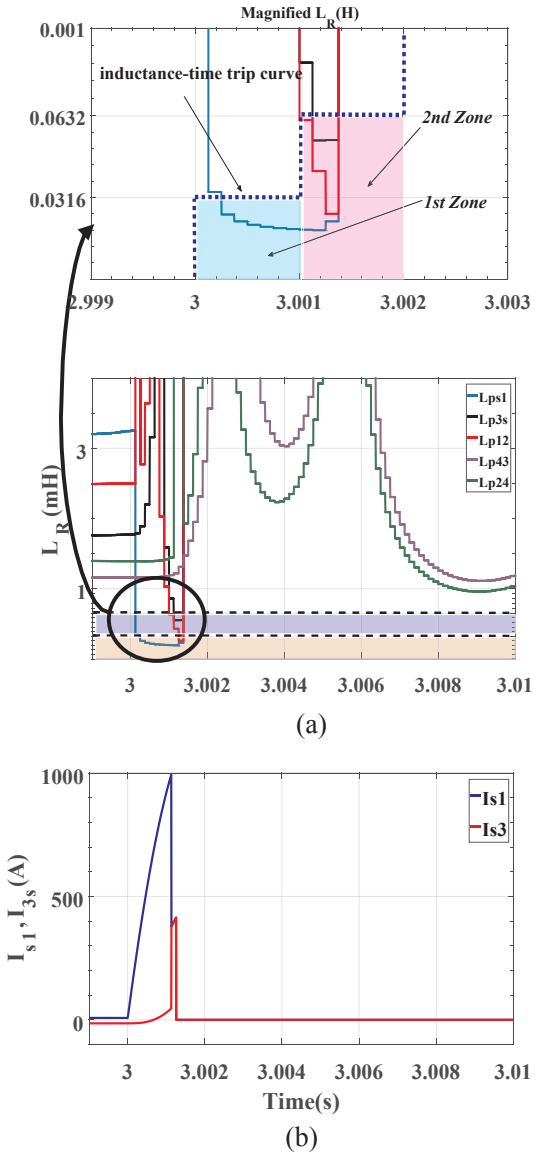

Fig. 11. Positive pole to ground fault f_4(a) estimated inductances byPD_{s1}, PD_{3s}, PD_{12},PD_{43} and PD_{24}, (b) s-1 and s-3 lines current.

inductance 0.223mH and 0.298mH, respectively; which are lower than fault detection threshold (Fig. 14a). Therefore, line 2–5 is disconnected by its protection units command and the fault current is suppressed within 0.2 ms (Fig. 14b). Also, as it is illustrated in Fig. 14a, the estimated inductances by protection units of the other lines are greater than the fault threshold.

3.8. Cyber-Physical risk assessment of the proposed protection scheme

A microgrid can be considered as a typical cyber-physical system. Cyber-system has being widely used in a microgrid which is often involved several geographically distributed units (such as protection and control units). They are coordinated based on the time, and highly dependent on the wide area communication. Therefore, protection units as part of a microgrid are extremely vulnerable against cyber-attacks, and significant damages and losses are possible [24]. Generally, side-channel analysis, distributed denial of service (DDoS), privacy leakage on the meter, malware and software flaws and theft of service are the main cybersecurity issues in the DC microgrids [25]. Since cyber-physical risk assessment are out of the scope of this paper, only the vulnerability of the proposed protection scheme against the main cybersecurity issues in DC microgrids is analyzed, and potential security solutions are provided in Table 4.

Side-channel analysis attacks are based on information extracted from the implemented processor units, rather than weaknesses in the implemented algorithm itself. Traffic camouflage can be used to countermeasure to the side-channel analysis. This approach transform the communication protocol of the measurements in the DC microgrid to an available one existed in the environment to prevent information hacking.

Internet Control Message Protocol (ICMP) attack is one of the DoS common attacks. In these attacks the ICMP requests with the targets IP address will be broadcasted. Most IP based devices, such as protection and control units accept the ICMP request. In this situation, it is possible for the attacker to take control of multiple targets. Since in the proposed protection scheme wide area network is eliminated, the possibility of such attacks are reduced.

Privacy leakage in measurement units generally is concerned to the remote collecting of the electricity usage data. Hence, it is independent from the protection algorithm. But eavesdropping of the microgrid situation and realizing load data give the attackers the opportunity of making creative attacks which would affect any part of the microgrid including protection system.

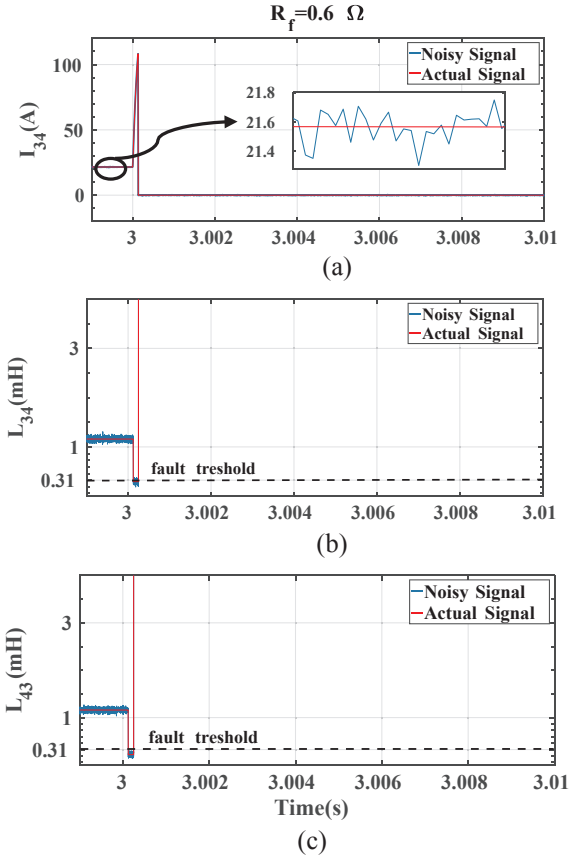

Fig. 12. Positive pole to ground fault f_5 withR_f = 0.6 Ω (a) line 3–4 current in noisy condition, (b) estimated inductances by PD_{34} (c) estimated inductances by PD_{43}.

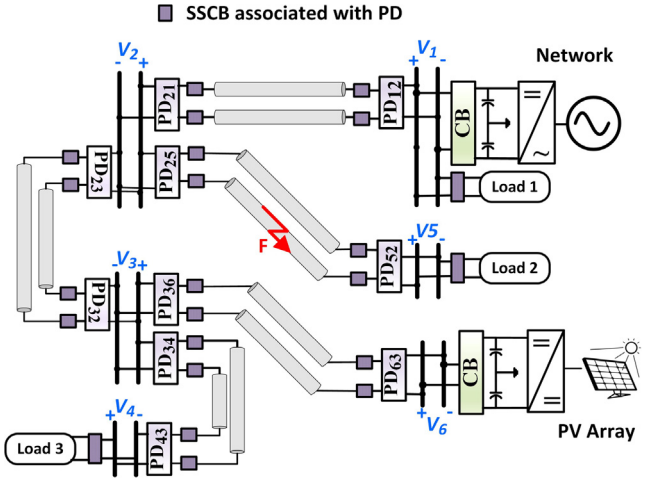

Fig. 13. Topology of DC distribution test system.

Furthermore, typically theft of service in the protection system can be considered as change in important protection scheme parameters or send false data from sensors or controllers to create hidden failures into the protection system; in this situation, to prevent unwanted events, false data injection attack can be detected and ignored using attack detection schemes such as [28]. Further investigation of cyber-physical attack in protection scheme based on local measurements in DC microgrids could be considered as future works for researchers.

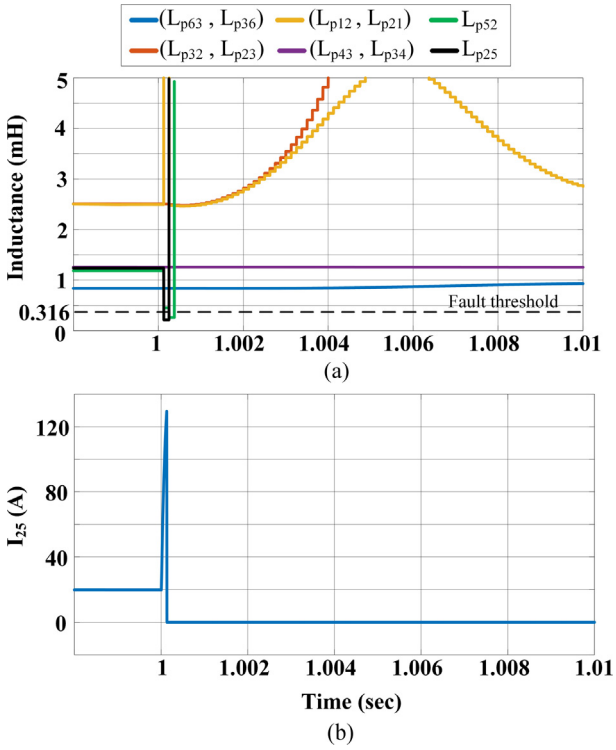

Fig. 14. Positive pole to ground fault f withR_f = 0.8 Ω (a) estimated inductances by DC distribution test system protection units, (b) line 2–5 current.

4. Comparison of the proposed protection scheme and previous studies

In this paper, a faulted line identification and isolation scheme (protection scheme) based on estimation of the fault path inductance is presented. To highlight the proposed approach advantages over earlier studies, first it is compared with schemes which are based on the parameters estimation (fault path inductance or resistance). Second, a comparison is made between the proposed protection scheme and other salient studies on LVDC microgrids.

4.1. Parameter estimation schemes comparison

Several papers have proposed methods to estimate fault path parameters to detect the fault and protect DC microgrids or locate the point of fault. Active impedance estimation (AIE) methods [30,31] are the most well-known among parameter estimation methods. In the AIE based scheme, once the faulty conditions are sensed, triangle current waveforms are injected by a power converter, and then the system impedance can be estimated at the point of coupling by processing the voltage and current responses. Although this approach locates the fault point with acceptable precision, it is not proper for faulted line identification and isolation and necessitates using a faster fault detection and isolation scheme to protect microgrids component. Furthermore, the implementation cost of this approach because of the additional power converter for triangular waveform injection is high. Another protection scheme which is based on estimation of fault path parameter (inductance) is proposed in [18]. In this method, the fault path inductance is estimated by linear least square method and also to increase selectivity a permission signal should be received by PDs from the other side of faulty line. Despite of the AIE scheme which is focused on locating the fault point, this approach like the proposed method of this paper has focused on faulted line identification and isolation. Even though this method has high selectivity, it still suffers from communication link dependency.

Table 4
Possible cybersecurity issues and solution in the proposed protection scheme.

Cybersecurity issue	Potential solution	Vulnerability of the protection scheme
side-channel analysis	Traffic Camouflage [26]	Depends to design and implementation
DDoS	DoS Attack Detection [27]	Low
privacy leakage on the meter	Balance between Security and Efficiency[25]	Moderate
malware and software flaws	Traffic Camouflage [26] Continues softwares monitoring and support	Depends to design and implementation
theft of service	False data injection attack detection schemes [28] Rootkit Countermeasure Traps[29]	Low

Table 5
Comparison of the proposed method with earlier studies.

studies	Scaled operation time (ms)	communication link existence	back-up protection	threshold robustness
this paper	≤0.2	✗	✓	✓
[10]	≤0.3	✓	✗	✗
[11]	≥0.5	✓	✗	✗
[18]	≥1	✓	✗	✓

4.2. Comparison of this paper method with salient previous studies

In Table 5, a comparison is made between earlier studies and the proposed protection scheme. All the studies are tested on the loop type microgrid of this paper, and the sampling frequency is set to 8 kHz. As can be seen, the proposed scheme has the shortest operation time among all salient previous studies. Furthermore, in order to increase reliability, the proposed scheme can provide back-up protection. The main advantages of the proposed scheme can be highlighted as short operation time, eliminating the need for the communication system and back-up protection. Another superiority of the proposed method is threshold robustness, which means that changes in microgrid topology including line outage, adding or removing power sources do not affect the predefined thresholds.

5. Conclusion

In this paper, protection scheme based on estimation of equivalent inductance for LVDC microgrids is proposed. Performance of the proposed scheme is investigated through various case studies. As shown in simulation results, the proposed method is able to detect any types of faults less than 0.2 ms. Selectivity is another advantage of the proposed method, which enables fault detection and isolation without disrupting operation of other parts. Although the presented fault detection is designed for fault resistance of 0.6 Ω, it is also tested for fault resistance of the 2 Ω fault where in both cases, the fault is detected very fast less than 0.2 ms. The defined inductance threshold of each PD only depends on inductance of the line to which PD is connected, thus any change in the microgrid topology does not affect the proposed scheme thresholds. Realization of backup protection is another advantage of the proposed fault detection which its performance is verified thoroughly under different fault scenarios. Furthermore, the simulation results demonstrated that the proposed protection scheme has the capability to be used in any other configurations. Eventually, a comprehensive comparison is made among earlier studies and superiority of the proposed method due to fast fault detection, communication-less operation, thresholds independency from microgrid topology and feasibility of back-up protection has illustrated.

Declaration of Competing Interest

The authors declare that they have no known competing financial interests or personal relationships that could have appeared to influence the work reported in this paper.

References

[1] Emhemed AAS, Burt GM. An advanced protection scheme for enabling an LVDC last mile distribution network. IEEE Trans Smart Grid 2014;5(5):2602–9.
[2] Manohar M, Koley E, Ghosh S. Enhancing resilience of PV-fed microgrid by improved relaying and differentiating between inverter faults and distribution line faults. Int J Electr Power Energy Syst 2019;108:271–9.
[3] Starke M, Tolbert LM, Ozpineci B. AC vs. DC distribution: a loss comparison. Transmission and Distribution Conference and Exposition, 2008. T&D. IEEE/PES; 2008. p. 1–7.
[4] Abdali A, Noroozian R, Mazlumi K. Simultaneous control and protection schemes for DC multi microgrids systems. Int J Electr Power Energy Syst 2019;104:230–45.
[5] Salomonsson D, Soder L, Sannino A. Protection of low-voltage DC microgrids. IEEE Trans. Power Deliv. 2009;24(3):1045–53.
[6] Stark MR, Li F, Tolbert LM, Ozpineci B. AC vs. DC distribution: maximum transfer capability. Proc. of IEEE Power and Energy Society General Meeting-Conversion and Delivery of Electrical Energy in the 21st Century. 2008. p. 1–6.
[7] Farhadi M, Mohammed O. Adaptive energy management in redundant hybrid DC microgrid for pulse load mitigation. IEEE Trans Smart Grid 2015;6(1):54–62.
[8] Naik J, Dhar S, Dash PK. Adaptive differential relay coordination for PV DC microgrid using a new kernel based time-frequency transform. Int J Electr Power Energy Syst 2019;106:56–67.
[9] Meghwani A, Srivastava SC, Chakrabarti S. A non-unit protection scheme for DC microgrid based on local measurements. IEEE Trans. Power Deliv. 2017;32(1):172–81.
[10] Farhadi M, Mohammed OA. Event-based protection scheme for a multiterminal hybrid DC power system. IEEE Trans Smart Grid 2015;6(4):1658–69.
[11] Emhemed AAS, Fong K, Fletcher S, Burt GM. Validation of fast and selective protection scheme for an LVDC distribution network. IEEE Trans. Power Deliv. 2017;32(3):1432–40.
[12] Saleh KA, Hooshyar A, El-Saadany EF. Hybrid passive-overcurrent relay for detection of faults in low-voltage DC grids. IEEE Trans Smart Grid 2017;8(3):1129–38.
[13] Fletcher SDA, Norman PJ, Fong K, Galloway SJ, Burt GM. High-speed differential protection for smart DC distribution systems. IEEE Trans Smart Grid 2014;5(5):2610–7.
[14] Dhar S, Dash PK. Differential current-based fault protection with adaptive threshold for multiple PV-based DC microgrid. IET Renew Power Gener 2017;11(6):778–90.
[15] Dhar S, Patnaik RK, Dash PK. Fault detection and location of photovoltaic based DC microgrid using differential protection strategy. IEEE Trans Smart Grid 2017;9(5):4303–12.
[16] Farhadi M, Mohammed OA. A new protection scheme for multi-bus DC power systems using an event classification approach. IEEE Trans Ind Appl 2016;52(4):2834–42.
[17] Monadi M, Gavriluta C, Luna A, Candela JI, Rodriguez P. Centralized protection strategy for medium voltage DC microgrids. IEEE Trans. Power Deliv. 2017;32(1):430–40.
[18] Mohanty R, Pradhan AK. Protection of smart DC microgrid with ring configuration using parameter estimation approach. IEEE Trans Smart Grid 2017;9(6):6328–37.
[19] Cairoli P, Dougal RA. Fault Detection and Isolation in Medium-Voltage DC Microgrids: Coordination Between Supply Power Converters and Bus Contactors. IEEE Trans Power Electron 2018;33(5):4535–46.
[20] Fletcher SDA, Norman PJ, Galloway SJ, Crolla P, Burt GM. Optimizing the roles of unit and non-unit protection methods within DC microgrids. IEEE Trans Smart Grid 2012;3(4):2079–87.
[21] Corless RM, Fillion N. A graduate introduction to numerical methods: From the viewpoint of backward error analysis. Springer; 2013.
[22] Carrica D, Benedetti M, Petrocelli R. Random sampling applied to the measurement of a DC signal immersed in noise. IEEE Trans Instrum Meas 2001;50(5):1319–23.
[23] Salonen P, Nuutinen P, Peltoniemi P, Partanen J. Protection scheme for an LVDC distribution system. Proc. EPE Conf. Power Elect. Appl. 2009.
[24] Wang C, Zhang T, Luo F, Li F, Liu Y. Impacts of cyber system on microgrid operational reliability. IEEE Trans Smart Grid 2017;10(1):105–15.
[25] Zhong X, Yu L, Brooks R, Venayagamoorthy GK. "Cyber security in smart DC microgrid operations. IEEE First International Conference on DC Microgrids (ICDCM), 2015. 2015. p. 86–91.
[26] Dyer KP, Coull SE, Ristenpart T, Shrimpton T. Protocol misidentification made easy with format-transforming encryption. Proceedings of the 2013 ACM SIGSAC

conference on Computer & communications security. 2013. p. 61–72.
[27] Özçelik İ, Brooks RR. Deceiving entropy based DoS detection. Comput Secur 2015;48:234–45.
[28] Beg OA, Johnson TT, Davoudi A. Detection of false-data injection attacks in cyber-physical DC microgrids. IEEE Trans Ind informatics 2017;13(5):2693–703.
[29] Hoglund G, Butler J. Rootkits: subverting the Windows kernel. Addison-Wesley Professional; 2006.
[30] Jia K, Christopher E, Thomas D, Sumner M, Bi T. Advanced DC zonal marine power system protection. IET Gener Transm Distrib 2014;8(2):301–9.
[31] Christopher E, Sumner M, Thomas DWP, Wang X, de Wildt F. Fault location in a zonal DC marine power system using active impedance estimation. IEEE Trans Ind Appl 2013;49(2):860–5.